Conceptual Model Analysis of the Influence of Temperature Feedbacks on Polar Amplification

Ashley E. Payne

August 16, 2015

1 Introduction

Polar amplification, the increased response of surface warming at high latitudes to radiative forcing relative to the global mean, is found in idealized models, paleoclimate records and in observations of the Arctic [3, 4, 7]. However, attribution of its causes is a complex problem because of the high degree of interaction between the different mechanisms at work.

Recent research has focused on the role of longwave feedbacks in polar amplification. Winton [2006] used twelve climate models from the fourth IPCC assessment report to compare the relative magnitudes of various feedbacks in the Arctic and globally for CO_2 doubling in 1%/year CO_2 increase experiments. He found that a large portion of the enhanced warming in the Arctic is attributable to the effect of longwave feedbacks, which include cloud, water vapor and temperature effects. Neutralizing the surface albedo feedback at high latitudes by replacing it by its global mean value in the feedback calculation still resulted in some degree of Arctic amplification relative to the global mean, indicating that the surface albedo feedback is important, but not dominant, in explaining polar amplification.

The temperature feedback can be broken into the Planck feedback, the background equilibrium response of the climate system, and the lapse rate feedback, the non-uniform change in temperature vertically. Both have been argued to be important to polar amplification in recent work. Pithan and Mauritsen [2014] performed a feedback analysis on data from phase 5 of the Coupled Model Intercomparison Project (CMIP5) and found that the temperature feedback dominates Arctic amplification, attributing this dominance to the interaction between the Planck feedback and the lapse rate feedback. Pithan and Mauritsen [2014] attribute a large part of the polar amplification to the Planck response itself, arguing that colder temperatures, as found at high latitudes relative to the low latitudes, require greater temperature increases for a given radiative forcing. The role of the lapse rate feedback in relation to the surface albedo feedback was investigated in Graversen et al. [2014] . By suppressing the lapse rate feedback in Community Climate System Model, version 4 (CCSM4) simulations, they found that a portion of polar amplification can be explained by its effect at high latitudes. However, the high level of interaction with the surface albedo feedback makes it difficult to consider the lapse rate independently.

The complexity of the problem highlights the importance of a simplified approach to gain insight into the roles of the Planck feedback and the lapse rate feedback on polar amplification. Here, we use a hierarchy of simple conceptual models to isolate the two different feedbacks and investigate whether (and if so, how much) polar amplification can be attributed to each.

As discussed in Pithan and Mauritsen [2014], the Planck feedback is indeed much weaker in the colder high-latitudes. However, we argue that this by itself cannot cause polar amplification. Instead, it is the qualitative difference in the lapse rate response between the low- and high-latitudes which is expected to contribute to polar amplification. While the low-latitude lapse rate is set by moist convection and is expected to decrease with increasing temperatures, leading to a negative lapse rate feedback, in the high-latitudes, models generally suggest a destabilization of the vertical temperature profile with warming [6], leading to positive lapse rate feedback.

The paper is organized as follows. In section 2, we describe our model setup, data, and method of quantifying feedback parameters. In section 3 we describe the radiative equilibrium response of surface temperature to increases in emissivity in a simple two-layer energy balance model. Against this equilibrium baseline, we investigate the Planck feedback and the lapse rate feedback in sections 4 and 5, respectively, using a hierarchy of models. In section 6, we look at the impact of these feedbacks on polar amplification, with and without the water vapor feedback. We summarize our results and future directions in section 7.

2 Data and Methods

2.1 Models

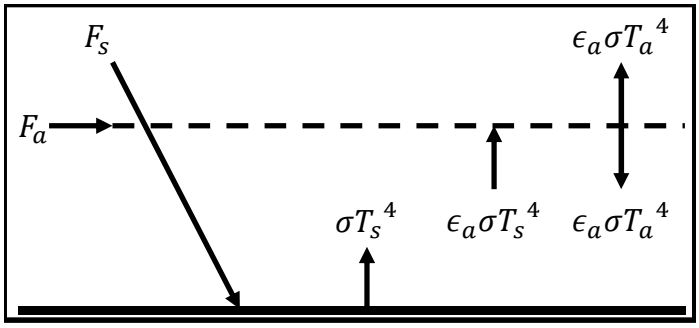

Figure 1: Illustration of a simple two-layer energy balance model with a surface layer and an atmospheric layer. F_s is the incoming solar radiation, F_a is atmospheric heat transport, T_s is the temperature of the surface layer, T_a is the temperature of the atmospheric layer, ϵ_a is the atmospheric emissivity and σ is the Stefan-Boltzmann constant.

We investigate the role of the longwave temperature feedback using a hierarchy of simple models. The simplest is a two-layer one-dimensional energy balance model (EBM), in which the system is represented by two layers; the bottom layer represents the planetary boundary layer and the top layer represents the free troposphere (Fig. 1). Energy input to the system

is in the form of solar insolation, F_s and meridional atmospheric heat transport, F_a, which can be turned on or off. The temperatures of the surface layer and the atmospheric layer are represented by T_s and T_a, respectively. The influence of increasing CO_2 concentration on warming is translated as increases in atmospheric emissivity, ϵ_a, which is assumed to be less than one.

For this simple model, we can write a system of equations that describe the balance of radiation in the two layers:

$$C_s \frac{dT_s}{dt} = F_s + \epsilon_a \sigma T_a^4 - \sigma T_s^4, \quad (1)$$

$$C_a \frac{dT_a}{dt} = F_a + \epsilon_a \sigma T_s^4 - 2\epsilon_a \sigma T_a^4, \quad (2)$$

where, C_s and C_a are the heat capacities of the surface and atmospheric layers, respectively.

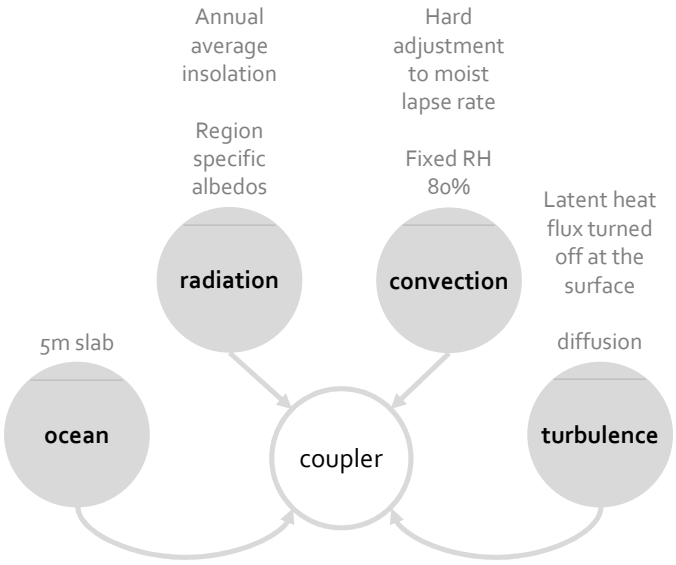

Figure 2: An illustration of the column model composed using the CliMT package, in which various components are linked through a coupler.

To step up complexity, we use a 26-layer radiative-convective column model. The model is based on the Climate Modelling and Diagnostics Toolkit (CliMT), available as a Python wrapper to various existing Fortran components [1]. Figure 2 describes the package set-up, in which ocean, radiation, convection and turbulence components interact using a coupler.

With the CliMT package we set up two different configurations. The first is a column model equivalent of the simple two-layer EBM described previously, in which a grey-gas radiative scheme is coupled to a slab ocean and a simple turbulence scheme. For this model, as well as for the simple two-layer EBM described previously, the role of water vapor is

not incorporated. The second model has an added level of complexity, with a multi-band radiative scheme based on the Column Radiation Model by the NCAR Community Climate Model (CCM3). In order to maintain the energy budget of the column model, but also to constrain the role of moisture, we turn off latent heat flux at the surface and fix relative humidity to 80% in the model troposphere and to zero in the model stratosphere.

When considered, convection is parameterized by hard adjustment to the moist adiabatic lapse rate. For each timestep, the temperature profile of the moist adiabatic lapse rate is calculated from the surface temperature. The intersection of this profile and the model-calculated temperature profile is found and all temperatures below that level are adjusted to the moist adiabat. The additional heat to the column due to this adjustment is pulled from the slab ocean and assumes efficient redistribution of heat from the surface throughout the column.

For the column model, in order to provide some level of comparison to the simple two-layer model, we use the average of the temperature profile between 500 and 600 hPa to represent the atmospheric temperature, T_a.

2.2 Data

We use ERA-Interim reanalysis to constrain parameter values in the following analysis, calculated as the climatological mean of the zonal average. In the following analysis, we will consider a "high-latitude" (HL) column and a "low-latitude" (LL) column. Parameter values for each of these columns are estimated based on ERA-Interim reanalysis data at 80°N and 20°N, respectively. An average insolation value of 367 W m^{-2} is used for non-region specific calculations.

To approximate the role of meridional atmospheric heat transport, we use the zonally averaged vertically integrated convergence of total energy flux (W m^{-2}) (Fig. 3a). In a given location, for the column models, we represent the atmospheric heating profile as a normal distribution that is capped at the tropopause and constrained to integrate to the value of total energy flux corresponding to its latitude, converted to units of K day^{-1} (Fig. 3b).

2.3 Feedback analysis

In order to quantify the contribution of the Planck and lapse rate feedbacks to changes in the surface temperature, we use the partial radiative perturbation method [9]. By this method, a feedback, λ_x, is represented as:

$$\lambda_x = \left(\frac{\partial R}{\partial x}\right)\left(\frac{\partial x}{\partial T_s}\right), \tag{3}$$

where R is the radiation at the top of the atmosphere (TOA) and T_s is the surface temperature. As our focus is on temperature feedbacks, Eqn. 3 becomes:

$$\lambda_T = \left(\frac{\partial R}{\partial T}\right)\left(\frac{\partial T}{\partial T_s}\right), \tag{4}$$

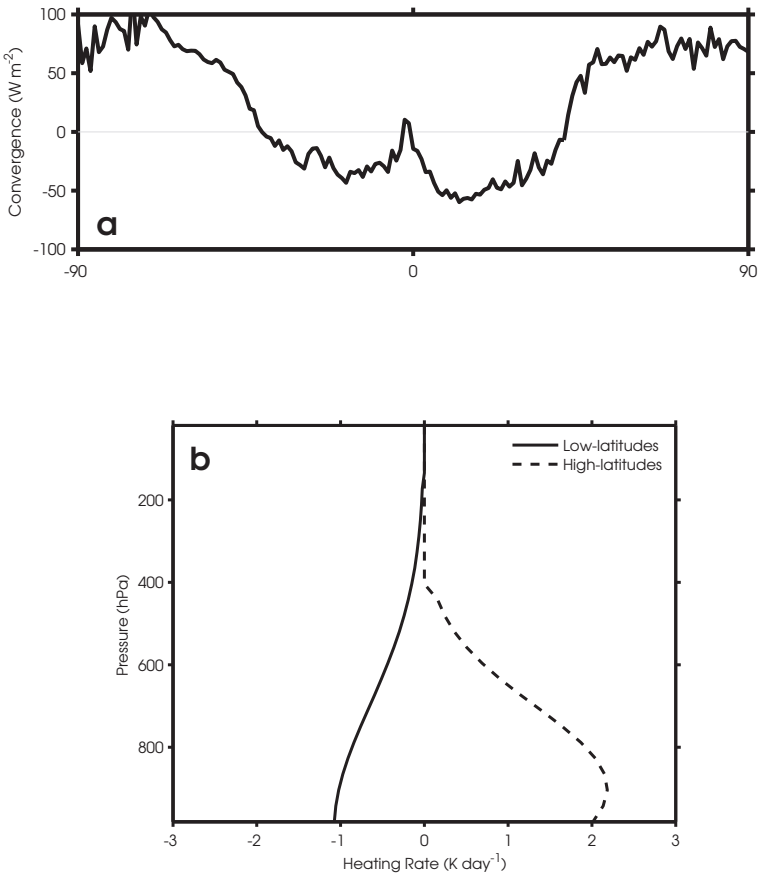

Figure 3: (a) Meridional variation of zonally averaged total energy flux calculated from ERA-Interim reanalysis (climatological mean over 1979 to 2013). (b) Heating rate profiles for the (solid line) low-latitudes and (dashed-line) high-latitudes in the column model.

and,

$$\lambda_T = \lambda_P + \lambda_{LR} \tag{5}$$

where λ_P is the Planck feedback and λ_{LR} is the lapse rate feedback.

In order to calculate the lapse rate feedback, we solve for the temperature feedback, λ_T and the Planck feedback, λ_P. The Planck feedback is the response of the TOA radiation budget in the absence of all other feedbacks and is based on the Stefan-Boltzmann law, so that the feedback is larger for higher temperatures. It is calculated as the derivative of the Stefan-Boltzmann equation and is negative as it dampens the temperature response to

perturbations in R by increasing the emission of longwave radiation[1]:

$$\lambda_P = -4\sigma T_e^3, \tag{6}$$

where, T_e is the effective emission temperature:

$$T_e = \frac{1}{\sigma}\left(F_s + F_a\right)^{1/4} \tag{7}$$

The temperature feedback, λ_T, is calculated as the TOA radiative response associated with the atmospheric and surface temperature changes, per degree of surface warming:

$$\lambda_T = \left(\frac{\partial R}{\partial T_a}\right)\left(\frac{\partial T_a}{\partial T_s}\right) + \left(\frac{\partial R}{\partial T_s}\right)\left(\frac{\partial T_s}{\partial T_s}\right), \tag{8}$$

where, from Fig. 1, the energy balance at the top of the atmosphere for OLR, R, can be written as:

$$R = -\epsilon_a \sigma T_a^4 - (1-\epsilon_a)\sigma T_s^4 \tag{9}$$

Taking the partial derivatives of Eqn. 9 with respect to T_a and to T_s and fitting them back into Eqn. 8, the temperature feedback is calculated as:

$$\lambda_T = -\left(4\epsilon_a \sigma T_a^3\right)\left(\frac{\partial T_a}{\partial T_s}\right) - 4\left(1-\epsilon_a\right)\sigma T_s^3 \tag{10}$$

so that:

$$\lambda_{LR} = -\left(4\epsilon_a \sigma T_a^3\right)\left(\frac{\partial T_a}{\partial T_s}\right) - 4\left(1-\epsilon_a\right)\sigma T_s^3 - \left(-4\sigma T_e^3\right) \tag{11}$$

3 Radiative equilibrium

Here, we consider the system in radiative equilibrium and the response of surface temperature to changes in emissivity. From Fig. 1, at equilibrium and assuming no atmospheric heat transport ($F_a = 0$), we can write the balance of radiation at the TOA as,

$$F_s = (1-\epsilon_a)\sigma T_s^4 + \epsilon_a \sigma T_a^4, \tag{12}$$

where, solving for the T_a term in Eqn. 1, we can simplify Eqn. 12 to:

$$2F_s = 2\sigma T_s^4 - \epsilon_a \sigma T_s^4 \tag{13}$$

We use $F_s = \sigma T_e^4$, to rewrite Eqn. 13 as:

$$T_e^4 = T_s^4 - \frac{1}{2}\epsilon_a T_s^4, \tag{14}$$

[1]The Planck response could alternatively be defined as the radiative response to vertically uniform warming. While not formally identical, the two definitions yield virtually the same results.

and substitute $\epsilon_a + \delta\epsilon_a$ and $T_s + \delta T_s$ for ϵ_a and T_s, respectively, into Eqn. 14,

$$T_e^4 = (T_s + \delta T_s)^4 - \frac{1}{2}(\epsilon_a + \delta\epsilon_a)(T_s + \delta T_s)^4 \tag{15}$$

To find the response of surface temperature to changes in emissivity, we solve Eqn. 15 for δT_s,

$$\delta T_s = \frac{T_s}{4(2 - \epsilon_a)}\delta\epsilon_a \tag{16}$$

At equilibrium, we can see from Eqn. 16 that the most basic state of the system shows that the change in surface temperature is proportional to the background state of surface temperature, T_s. For a given change in emissivity, assumed to be globally constant, we can compare the response of the high-latitudes (HL) and low-latitudes (LL):

$$\frac{\delta T_s^{HL}}{T_s^{HL}} = \frac{\delta T_s^{LL}}{T_s^{LL}} \tag{17}$$

We, therefore, expect a somewhat larger change in low-latitude surface temperature, δT_s^{LL}, relative to the change in high-latitude surface temperature, δT_s^{HL}, because of the greater initial temperatures (in general) in the low-latitudes relative to the high-latitudes. Thus, for this radiative equilibrium state, amplification of surface temperatures occurs in the tropics rather than at high-latitudes. Tropical amplification is evident in solutions to Eqns. 1 and 2 at equilibirum. Figure 4 shows the difference in surface temperatures for a (blue) high- and (orange) low-latitude column.

4 The Planck feedback

The radiative equilibrium response discussed above implies a change in the lapse rate. To isolate the effect of the Planck feedback on the surface temperature response to changing emissivity, we consider a configuration of the two-layer EBM with a fixed lapse rate, in which the temperature of the atmospheric layer is dependent on the surface temperature. We present a perturbation analysis of surface temperature to changes in emissivity in section 4.1 and in section 4.2, we compare the solution for the two-layer experiment to its equivalent in the column grey-gas model. For this section, we use an average insolation value of 367 W m^{-2}.

4.1 Fixed lapse rate

Modifying the setup in section 3, we fix the lapse rate, so that the change in temperature with height is a constant, ΔT_c. As in section 3, we perform a perturbation analysis using the simple two-layer EBM, but with the added constraint:

$$T_a = T_s - \Delta T_c, \tag{18}$$

which we fit into Eqn. 12 and, using the definition of F_s, get:

$$T_e^4 = (1 - \epsilon_a)T_s^4 + \epsilon_a(T_s - \Delta T_c)^4 \tag{19}$$

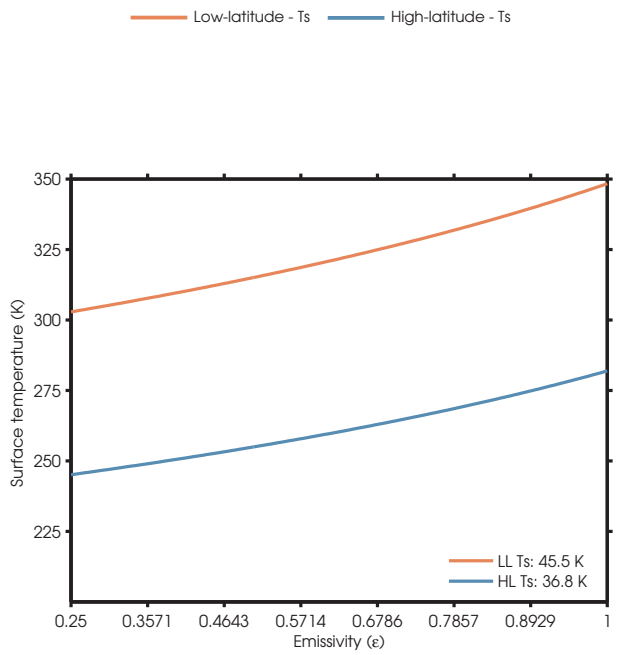

Figure 4: Comparison between solutions for the two-layer model between (orange) low-latitude surface temperature and (blue) high-latitude surface temperature response to increasing emissivity, where the legend indicates the total change in T_s for each region.

As in section 3, we are interested in the surface temperature response to changing emissivity. Thus, we substitute $\epsilon_a + \delta\epsilon_a$ and $T_s + \delta T_s$ for ϵ_a and T_s, respectively, in Eqn. 19:

$$T_e^4 = (1 - (\epsilon_a + \delta\epsilon_a))\,(T_s + \delta T_s)^4 + (\epsilon_a + \delta\epsilon_a)\,((T_s + \delta T_s) - \Delta T_c)^4 \tag{20}$$

Linearizing and ignoring higher order terms (where we assume T_s is much greater than the perturbation terms), we are left with:

$$4\epsilon_a T_s^3 \delta T_s - 4\epsilon_a (T_s - \Delta T_c)^3 \delta T_s - 4T_s^3 \delta T_s = \delta\epsilon_a (T_s - \Delta T_c)^4 - \delta\epsilon_a T_s^4 \tag{21}$$

Solving Eqn. 21 for δT_s:

$$\delta T_s = \frac{(T_s - \Delta T_c)^4 - T_s^4}{4\epsilon_a (T_s^3 - (T_s - \Delta T_c)^3) - 4T_s^3} \delta\epsilon_a \tag{22}$$

Assuming that ΔT_c is much less than T_s we can simplify Eqn. 22 to:

$$\delta T_s \approx \Delta T_c \delta\epsilon_a \tag{23}$$

Equation 23 shows that the change in surface temperature is proportional to the magnitude of the lapse rate, ΔT_c. Thus, for a given lapse rate we do not expect amplified surface

warming at high latitudes based on the differential Planck response alone. Instead, we may expect reduced warming in the high-latitudes, due to the typically small lapse rate found there.

4.2 Comparison to column model and feedback analysis

We extend the analysis in section 4.1 to the column model with a grey-gas radiative scheme, as described in section 2.1. Results for the column model are qualitatively similar to those of the two-layer model. Figures 5a and 5b show a comparison between the response of (grey line) atmospheric temperature to increasing atmospheric emissivity relative to (black line) surface temperature, in (solid) radiative equilibrium and with (dashed) a fixed lapse rate, for the two-layer and column grey gas models, respectively. For the fixed lapse rate solution, ΔT_c is adjusted so that the atmospheric temperature at an emissivity of 0.3 is equal to the temperature of the radiative-equilibrium solution in each model and approximates the dry adiabatic lapse rate.

The results discussed above may seem to be at odds with the notion that the Planck feedback ought to be weaker at high-latitudes. The reason for the lack of enhanced warming lies in the similarly weaker radiative forcing, associated with a given increase in the optical thickness of the atmosphere. The effect of the Planck feedback in modifying radiative forcing is seen in Fig. 6a, which shows the radiative forcing for the (solid) radiative equilibrium state and (dashed) fixed lapse rate case for the two-layer EBM. Due to our use of a constant Planck feedback calculation, the slight residual difference between the radiative forcing and Planck feedback is manifested as a small lapse rate feedback, even for the fixed lapse rate case. For comparison, Fig. 6b shows the (black) fixed lapse rate radiative forcing seen in Fig. 6a plotted with the radiative forcing for fixed lapse rate in the (blue) high- and (orange) low-latitudes. At higher emissivity, the larger lapse rate for the radiative equilibrium state shows the larger radiative forcing.

5 Lapse rate changes and feedbacks

Here, we include the role of meridional atmospheric heat transport to investigate its role in setting the sensitivity of the lapse rate feedback to changes in atmospheric emissivity. We consider two cases: (1) a system in radiative-dynamic equilibrium, that is with the lapse rate controlled by the interaction of radiation and a prescribed atmospheric heat transport, and (2) a system with a convective lapse rate in the low-latitudes. As atmospheric heat transport changes sign in the meridional direction, we now consider two columns for each experiment: (1) a high-latitude column and (2) a low-latitude column.

5.1 Two-layer EBM

5.1.1 Radiative equilibrium

For a small change in atmospheric emissivity, $\delta\epsilon_a$, we assume a small change in the surface temperature, δT_s, and the atmospheric temperature, δT_a. How amplification will affect meridional heat transport is an active area of research, however, to isolate out the effects

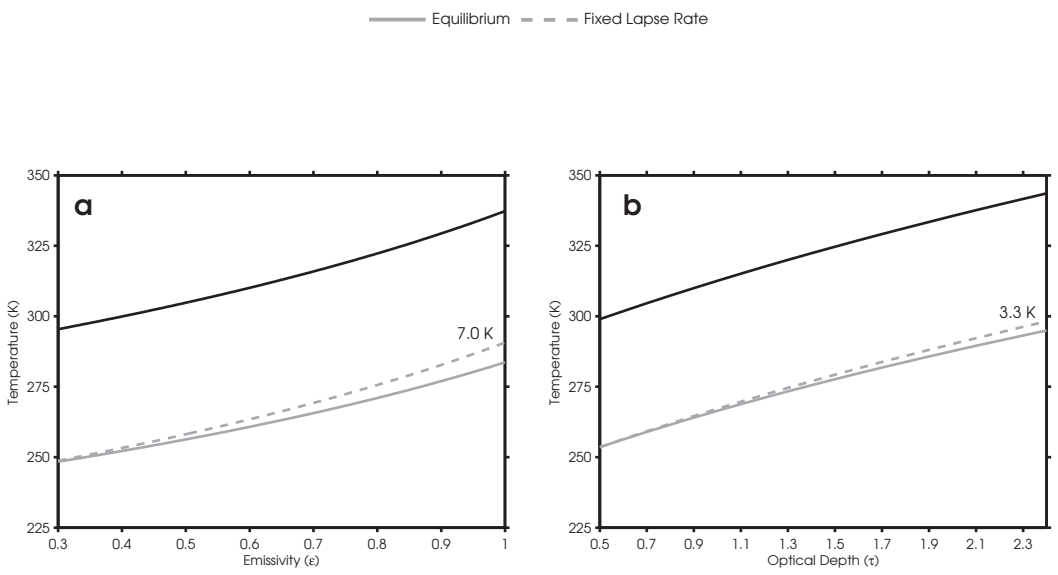

Figure 5: Comparison between solutions for the (a) two-layer model and (b) column grey-gas model showing the trend in (black line) surface and (grey line) atmospheric temperatures for the (solid line) radiative equilibrium and (dashed line) fixed lapse rate experiments.

of local feedbacks versus changes in the heat transport, we will assume a constant heat transport which is unaffected by changes in emissivity. At equilibrium, with these small changes, Eqn. 2 becomes,

$$F_a + (\epsilon_a + \delta\epsilon_a)\sigma(T_s + \delta T_s)^4 = 2(\epsilon_a + \delta\epsilon_a)\sigma(T_a + \delta T_a)^4 \tag{24}$$

Linearizing Eqn. 24 and ignoring higher order terms, leaves us with an expression for the response of the lapse rate to a change in emissivity,

$$8\epsilon_a\sigma T_a^4\left(\frac{\delta T_a}{T_a} - \frac{\delta T_s}{T_s}\right) = -F_a\left(\frac{\delta\epsilon_a}{\epsilon_a} + 4\frac{\delta T_s}{T_s}\right) \tag{25}$$

For a positive atmospheric heat flux convergence, where $F_a > 0$, the L.H.S. of Eqn. 25 must be negative, and thus $\delta T_a/T_a < \delta T_s/T_s$. Since generally $T_s > T_a$, this implies that $\delta T_a < \delta T_s$ and, thus, an increase in the lapse rate. If the atmospheric heat flux convergence is negative (i.e. $F_a < 0$), we may instead expect a decrease in the lapse rate.

Due to the meridional differences in the energy balance between incoming solar insolation and outgoing longwave radiation, the low-latitudes are characterized by a net export of heat and the high-latitudes are characterized by a net import of heat. This can be seen in Fig. 3. Based on Eqn. 25, we, therefore, expect to see a greater increase in surface temperatures relative to atmospheric temperatures in the high-latitudes (an increase in the lapse

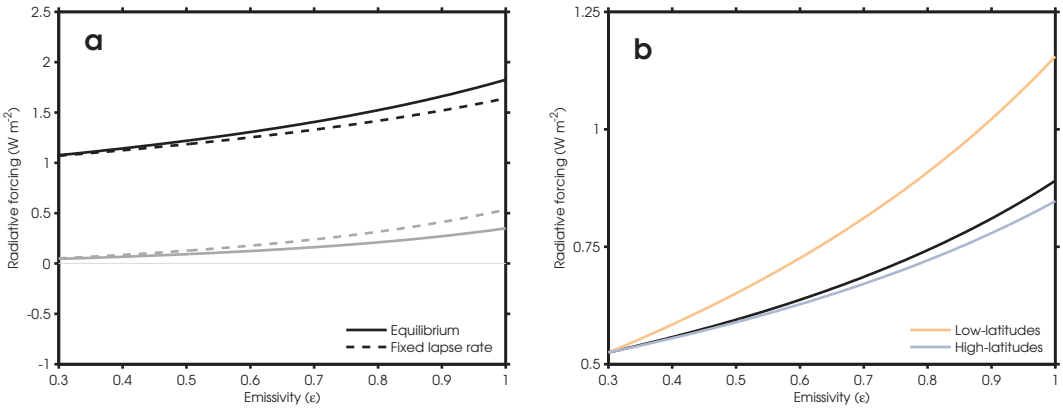

Figure 6: For the two-layer EBM, (a) comparison between the (black) radiative forcing and the (grey) lapse rate feedback for the (solid line) radiative equilibrium and (dashed line) fixed lapse rate experiments. (b) Comparison of the radiative forcing between the (blue) high- and (orange) low-latitudes with the (black) radiative forcing for the fixed lapse rate experiment.

rate). For the tropics, the radiative-dynamic equilibrium solution in Eqn. 25, would instead suggest a decrease in the lapse rate. However, the radiative-dynamic equilibrium solution is also statically unstable in the tropics, which would trigger convection. In practice, Eqn. 25 is thus not applicable in the tropics, where the lapse rate is set by convection.

We compare solutions of T_s and T_a for the high-latitude column to a convective low-latitude column in the next section. The system of equations for the high-latitudes are then (from Eqns. 1 and 2, at equilibrium):

$$T_s = \left[\frac{F_a + 2F_s}{2\sigma - \epsilon_a\sigma}\right]^{1/4}, \tag{26a}$$

$$T_a = \left[\frac{F_a + \epsilon_a F_s}{2\epsilon_a\sigma - \epsilon_a^2\sigma}\right]^{1/4}, \tag{26b}$$

5.1.2 Convective lapse rate

We add a level of realism to our two-layer model by allowing the lapse rate in the low-latitude scenario to be set by convection. In the low-latitudes, where the lapse rate is set by convection, the two-layer system is described by the energy balance at the TOA and by a temperature dependent lapse rate:

$$F_s + F_a = (1 - \epsilon_a)\sigma T_s^4 + \epsilon_a\sigma T_a^4, \tag{27a}$$

$$T_a = T_s - \Delta T \tag{27b}$$

In contrast to section 4.1, ΔT is not constant, but is dependent on the moist adiabatic lapse rate, Γ_w,

$$\Gamma_w = g\frac{1+{}^{L_v r}/_{R_d T}}{C_{pd}+{}^{L_v^2 r}/_{R_v T^2}}, \tag{28}$$

where L_v is the latent heat of vaporization, R_d is the specific gas constant of dry air, C_{pd} is the heat capacity of dry air at constant pressure, and R_v is the specific gas constant of water vapor. Since the amount of moisture is dependent on temperature, the mixing ratio of the mass of water vapor to that of dry air, r changes with temperature and pressure:

$$r = {}^{0.622 e_s}\,/_{(P-e_s)}, \tag{29}$$

where e_s is the saturation vapor pressure:

$$e_s = 6.11 \exp \frac{L_v}{R_v}\left(\frac{1}{273}-\frac{1}{T}\right) \tag{30}$$

The atmospheric temperature is assumed to be at 500 hPa and is calculated by integrating the change in temperature, T, along the moist adiabatic lapse rate profile with height.

5.2 Comparison to column model and feedback analysis

Here, we compare the solutions of the two-layer EBM to those from the column grey-gas model. The column grey-gas model is setup for the same two cases as the two-layer model: (1) a radiative-dynamic equilibrium case, and (2) a case with a radiative-convective column in the low-latitudes.

5.2.1 Role of atmospheric heat transport

In this section, we want to examine the effect of atmospheric heat transport on the radiative-dynamic equilibrium solution. We are thus assuming a radiative-dynamic equilibrium solution also for the low-latitude column, ignoring the effects of convection. The more realistic case with a convective lapse rate in the tropical column is discussed in section 5.2.2.

The interpretation of Eqn. 25 in section 5.1.1 is supported by solutions for the two-layer EBM and the column grey-gas model. Figure 7 shows a comparison of the temperature response to changes in optical thickness for the (solid lines) radiative equilibrium and (dashed lines) radiative-dynamic equilibrium for the (a,c) two-layer model and (b,d) column grey-gas model. Temperature trends for the two models are very similar and consistently show an increase in the lapse rate with the introduction of heat transport, evident in the flattening of the atmospheric temperature trend in Figs. 7c and 7d. In the high-latitudes, the lapse rate of the radiative-dynamic equilibrium state increases with increasing optical thickness. The opposite occurs at low-latitudes.

While there is a large response in the lapse rate to atmospheric heat transport, the surface temperature response still shows a slightly higher increase in low-latitude surface temperatures relative to high-latitude temperatures. Introduction of heat transport to the models

slightly reduces the amount of surface heating in the low-latitude scenario and slightly increases the surface heating in the high-latitudes. However, the models still show amplification of low-latitude surface temperature relative to the high-latitudes.

Focusing on the high-latitudes where there is a large response to atmospheric heating, Fig. 8 shows the radiative response (the product of the total surface temperature change with the feedback parameter) of the Planck and lapse rate feedbacks to changes in emissivity at high latitudes for the two experiments (a) without and (b) with atmospheric heat transport. As inferred from Fig. 7, the magnitude of the lapse rate feedback is larger in the presence of atmospheric heat transport. However, the dynamic heat transport also strongly changes the radiative forcing by changing the lapse rate of the background state, as discussed in section 4.1. The effect of the dynamic heat transport on the base-state lapse rate, and thus the radiative forcing, here approximately cancels the effect of the lapse rate feedback. For the high-latitude atmospheric temperature response, near $\epsilon_a = 0.3$ in Fig. 8, the radiative forcing changes sign from negative (cooling) to positive (warming). This change in sign is associated with a change in sign of the lapse rate, which for a small epsilon is very efficiently stabilized by the atmospheric heat transport.

5.2.2 Effect of convection on low-latitude temperature response

In the previous section, no polar amplification was evident due to the amplified response of the low-latitudes to increases in atmospheric emissivity (or optical depth). In order to investigate the effect of convection on the comparative role of the low-latitudes to the high-latitudes and polar amplification, we compare the temperature response at low-latitudes, with active heat transport, with- and without- convection in the two models (Fig. 10). Two processes must be taken into account to adequately explain the figure: (1) the role of convection on the lapse rate of the background state and (2) the negative lapse rate feedback set by moist convection.

Figure 9 shows the same as Fig. 8, but for the (a) non-convective and (b) convective low-latitudes. Comparison of the two panels shows a large decrease in the amount of radiative forcing for a given change in emissivity. The role of convection in the tropics acts to decrease the lapse rate of the background state. This reduction results in the large decrease of radiative forcing, as discussed in section 4.1. Superimposed on its influence on the background state lapse rate, convection also imposes a negative lapse-rate feedback in the tropics, as the moist adiabatic lapse rate decreases with increasing temperature. Figure 9b shows an increasingly negative lapse rate feedback with increasing emissivity, associated with the increase in the lapse rate feedback with rising temperature (causing an exponential rise in the saturation specific humidity).

The reduction of the radiative forcing and the negative lapse rate feedback, resulting from the addition of moist convection, have strong implications for the sensitivity of the surface temperature with increasing optical thickness. Figure 10 shows the weakening of the tropical surface temperature response when convection is taken into account. Compared to the almost constant lapse rate in Fig. 7, there is a large decrease in the lapse rate, which is

reflected in the feedback analysis.

6 Impact on polar amplification

6.1 Dry longwave perspective

Here, we bring together the results from previous sections to compare the high- and low-latitude columns in the two-layer EBM and column grey-gas models in order to investigate their impact on polar amplification. We use a low-latitude scenario with a convective lapse rate and negative heat transport and a high-latitude scenario with a lapse rate set by radiation and positive heat transport.

Figures 11a and 11b show temperature trends for the two-layer model and column grey-gas model, respectively. Both models show an amplification of surface temperatures in the high-latitudes relative to the low-latitudes. This amplification is associated with a large increase in the high-latitude lapse rate, as opposed to a decrease in the low-latitude lapse rate, which can be seen in Fig. 11c and 11d, where the response of lapse rate in each region is plotted against emissivity. These results are in line with the perturbation analysis in section 5 and provide evidence for the role of the lapse rate feedback in modifying the sensitivity of surface temperature to changes in emissivity (or optical thickness).

The amplification of polar surface temperatures relative to the tropics implies a weakening of the surface temperature gradient. In the free troposphere, the opposite case is found, where polar atmospheric temperatures increase at a smaller rate than tropical atmospheric temperatures, in line with the sign of the lapse rate feedback response in each region. The difference in the warming pattern between the surface and atmosphere in the two regions is a robust feature found in previous research [8] and has implications on mid-latitude dynamics and changes in the atmospheric heat transport with warming.

6.2 The role of water vapor and heat transport

The analysis in the previous sections focused on the roles of the Planck and lapse rate feedbacks in a dry atmosphere. Here, we use a multi-band radiative transfer scheme based on CCM3 in the column model, and allow for changes in specific humidity. For simplicity, the relative humidity is held fixed at 80%. We will compare temperature trends between a convective low-latitude scenario and a high-latitude scenario, both with atmospheric heat transport.

Figure 12a shows the temperature trends for the column model, with the absolute temperature shifted such that the atmospheric temperature is the same as the surface temperature at 280 ppmv for better comparison. The results indicate that the more realistic column model is in agreement with the lapse rate results from the simpler models, where lapse rate increases in the high-latitudes and decreases in the low-latitudes. However, amplification of polar surface temperatures is no longer evident relative to low-latitude surface temperatures. Surface warming in the low-latitudes is almost double that at high-latitudes.

The difference between the results in section 6.1 and those in Fig. 12a is directly attributable to the the presence of the water vapor feedback. To isolate this feedback, we fix the vertical specific humidity profile to their value at 380 ppmv. We then compare the low-latitude surface temperatures for this fixed scenario to one in which water vapor instead responds to increasing CO_2 concentrations. Figure 12b shows the difference in low-latitude surface temperatures for the two experiments. Suppressing the WV feedback leads to a suppression of surface temperature warming in the convective tropics and the re-emergence of polar amplification. Without the water vapor feedback, the model behaves similarly to the results described in section 6.1, using a grey-gas radiative transfer scheme or the EBM. However, with an approximately constant relative humidity in the models, the water vapor feedback results in a strongly enhanced tropical warming, while having little effect at high latitudes. This cancels the differential effect of the lapse rate feedback, and instead leads to low-latitude amplification. Additional feedbacks (such as ice-albedo or clouds) and /or changes in the atmospheric heat transport are, thus, likely to be necessary to explain polar amplification in Earth's atmosphere and in GCMs.

7 Summary and conclusions

In this project, we used a hierarchy of conceptual models of increasing complexity to test the roles of the Planck feedback and the lapse rate feedback in polar amplification. Using a simple column model with a fixed lapse rate, we argue that the Planck feedback alone cannot explain polar amplification. Instead, the surface warming expected for a given change in atmospheric optical thickness depends primarily on the prescribed lapse rate itself (but not on the temperature of the base state). While the strength of the Planck feedback does increase with the temperature of the base state, the effective radiative forcing, associated with a given change in atmospheric optical thickness, increases approximately similarly with the base state temperature. As a result, the net warming for a given change in atmospheric optical thickness is approximately independent of the base state temperature. The differing response of the lapse rate at high- and low-latitudes instead does cause polar amplification. At high latitudes, the lapse rate is sensitive to atmospheric heat transport and increases strongly in response to increasing atmospheric optical thickness.

When we consider the role of water vapor in our column model by using a multi-band radiative transfer scheme, and holding atmospheric relative humidity constant, low-latitude surface temperatures changes in response to CO_2 increases are amplified relative to high-latitude surface temperature changes. This indicates that the stronger water vapor feedback in the tropics cancels the polar amplification associated with the lapse rate feedback. To isolate the role of water vapor, we fix water vapor to 380 ppmv for a range of CO_2 concentrations. With the water vapor feedback essentially removed, high latitude surface temperatures are again amplified relative to low-latitude surface temperatures. These results suggest that, while the lapse rate feedback does play a role in Arctic amplification of surface temperatures, the effect is masked in comparison by the large water vapor feedback at low latitudes.

Future work for this project includes:

- The calculation of feedback parameters for the column models for better comparison to the results of the two-layer model experiments. This task is important for quantifying the role of the lapse rate feedback in the higher order models. In addition, we can use feedback analysis in the realistic radiative scheme column model to investigate the role of the water vapor feedback in relation to the Planck and lapse rate feedbacks.
- The parameterization of a dynamic heat transport between the high- and low-latitudes in the two-layer EBM and column models. In the current setup, the two regions are completely decoupled and used only for comparison. Our results suggest a decrease in the meridional temperature gradient at the surface and an increase in the gradient in the free troposphere. This has implications on dynamic heat transport in the mid-latitudes.

8 Acknowledgements

I would like to thank Malte Jansen for giving me the opportunity to work on this interesting problem for the summer. He was an excellent advisor and I am very grateful for his incredible patience with me. I truly enjoyed my experience in the program and would like to thank the directors, main lecturers and all others I had the opportunity to talk to over the course of the summer for their insight.

References

[1] R. Caballero and M. Steder, *Climt: An object-oriented climate modelling and diagnostics toolkit* `http://maths.ucd.ie/~rca/climt/`, 2008.

[2] R. G. Graversen, P. L. Langen, and T. Mauritsen, *Polar amplification in CCSM4: Contributions from the lapse rate and surface albedo feedbacks*, Journal of Climate, (2014), pp. 4433 – 4450.

[3] S. Manabe and R. J. Stouffer, *Sensitivity of a global climate model to an increase of CO_2 concentration in the atmosphere*, Journal of Geophysical Research, 85 (1980), pp. 5529-5554.

[4] G. H. Miller, R. B. Alley, J. Brigham-Grette, J. J. Fitzpatrick, L. Polyak, M. C. Serreze, and J. W. White, *Arctic amplification: can the past constrain the future?*, Quaternary Science Reviews, 29 (2010), pp. 1779 – 1790.

[5] F. Pithan and T. Mauritsen, *Arctic amplification dominated by temperature feedbacks in contemporary climate models*, Nature Geoscience Letters, 7 (2014), pp. 181-184.

[6] M. Serreze, A. Barrett, J. Stroeve, D. Kindig, and M. Holland, *The emergence of surface-based Arctic amplification*, The Cryosphere, 3 (2009), pp. 11 – 19.

[7] S. Solomon et al., eds., *Climate Change 2007: The Physical Science Basis*, Cambridge University Press, 2007.

[8] ——, *Climate Change 2007: The Physical Science Basis, Ch. 10*, Cambridge University Press, 2007.

[9] R. Wetherald and S. Manabe, *Cloud feedback processes in a general circulation model*, Journal of Atmospheric Sciences, 45 (1988), pp. 1397 – 1415.

[10] M. Winton, *Amplified arctic climate change: What does surface albedo feedback have to do with it?*, Geophysical Research Letters, 33 (2006).

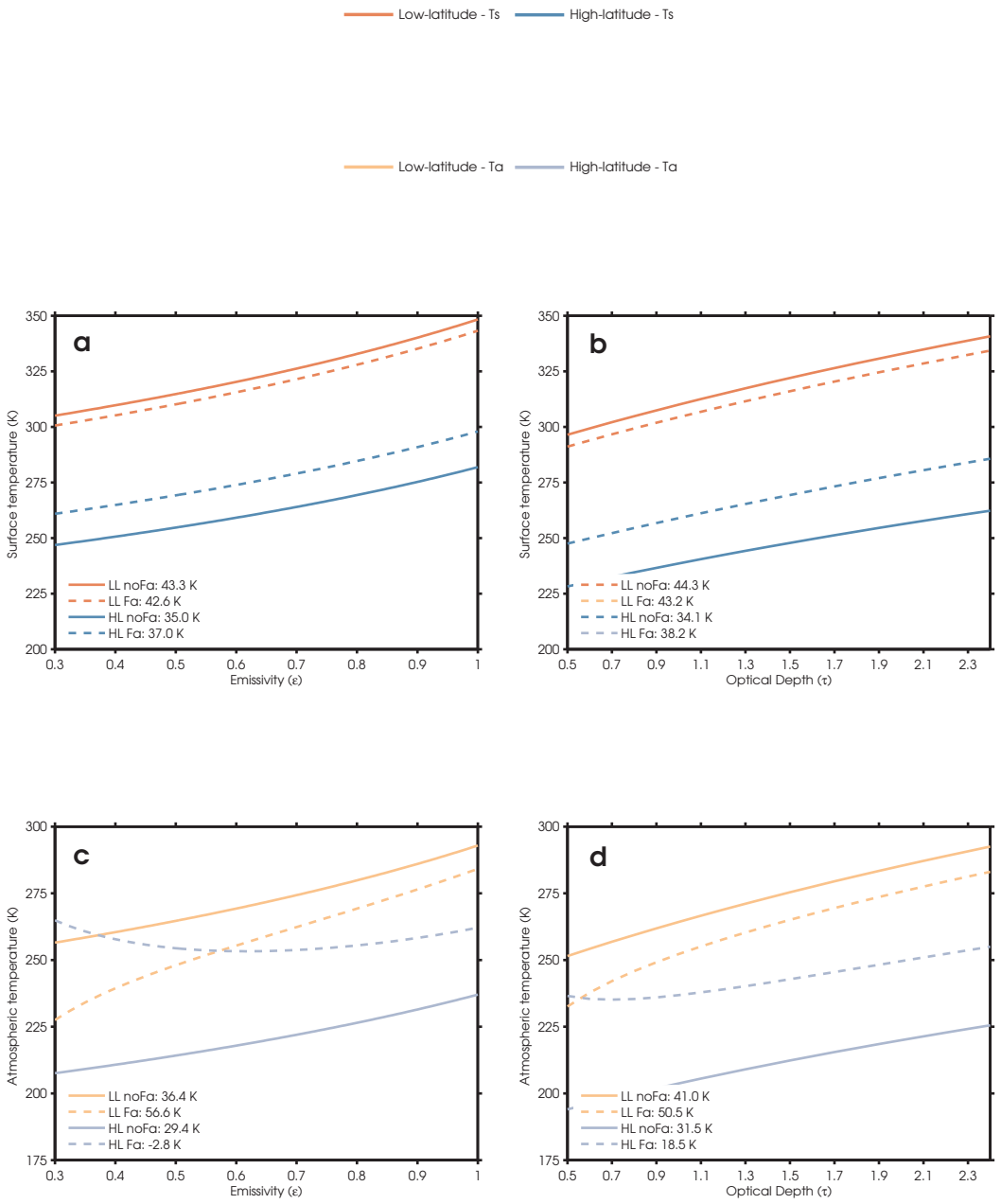

Figure 7: (a,b) Surface temperature and (c,d) atmospheric temperature response to increasing emissivity for the (orange) low-latitudes and (blue) high-latitudes, (solid line) without and (dashed line) with atmospheric heat transport for the (a,c) two-layer EBM and (b,d) column grey-gas model. The numbers in the legends of each panel show the temperature change between the thickest atmospheric limit and the thinnest limit for each scenario.

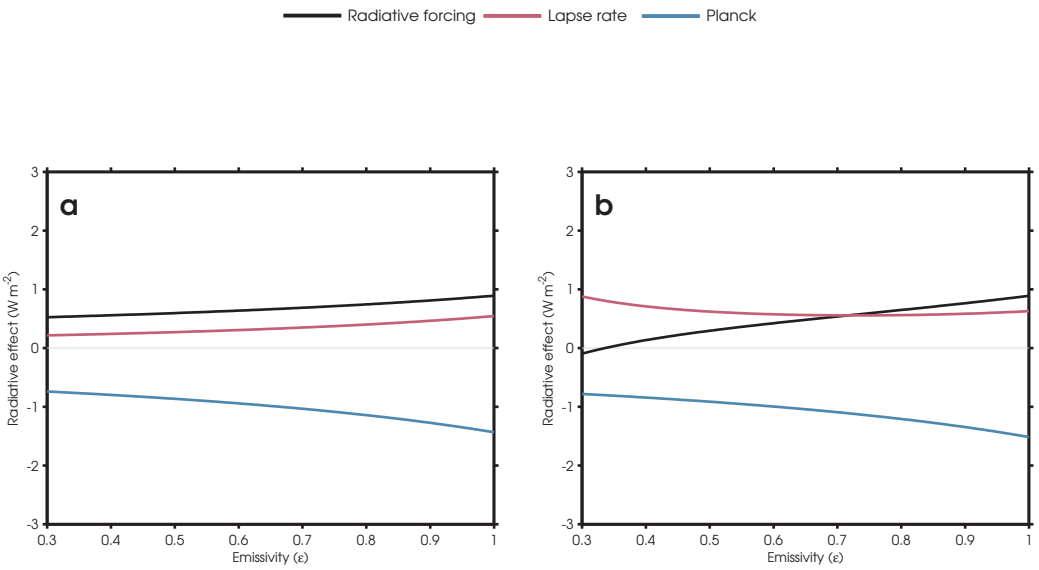

Figure 8: At high-latitudes, the radiative response of the (blue) Planck feedback and the (pink) lapse rate feedback to (black) radiative forcing (a) without atmospheric heat transport and (b) with atmospheric heat transport.

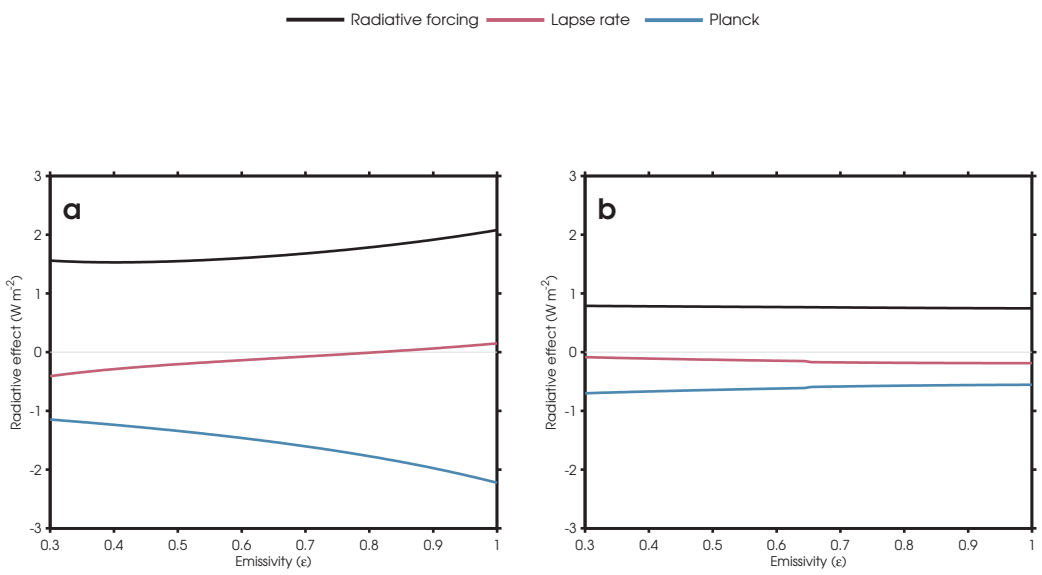

Figure 9: At low-latitudes, the radiative response of the (blue) Planck feedback and the (pink) lapse rate feedback to (black) radiative forcing (a) without and (b) with convection.

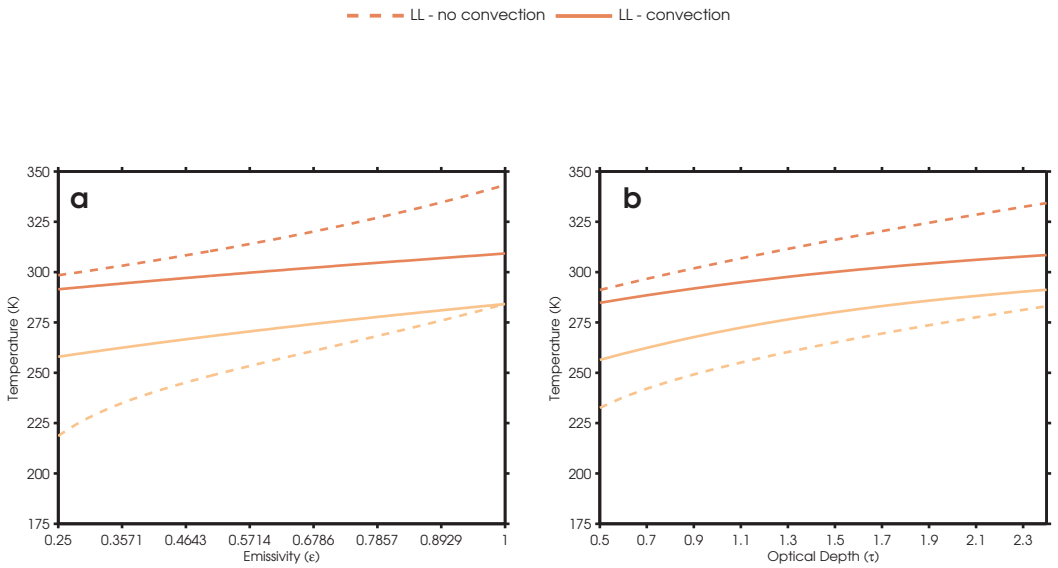

Figure 10: Comparison between (dark orange) surface temperature and (light orange) atmospheric temperature (solid line) without convection and (dashed line) with convection for the (a) two-layer EBM and (b) column grey-gas model.

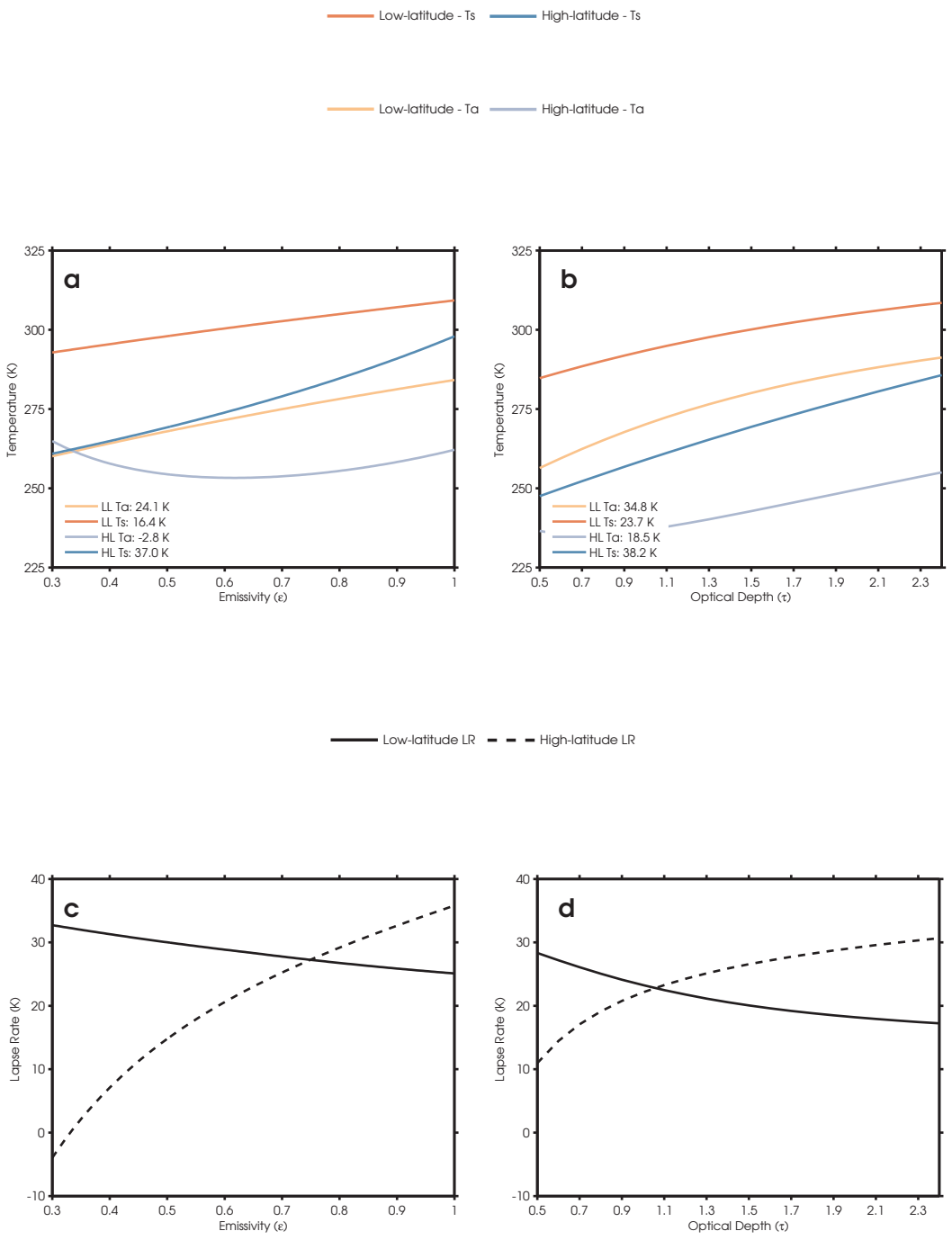

Figure 11: For the (a,c) two-layer EBM and the (b,d) column grey-gas model, (a,b) Surface temperature and atmospheric temperature response to increasing emissivity (optical depth) and (c,d) lapse rate changes for the (blue, black dashed) high- and (orange, black solid) low-latitude scenarios. The numbers in the legends of panels (a) and (b) are the same as in Fig. 7

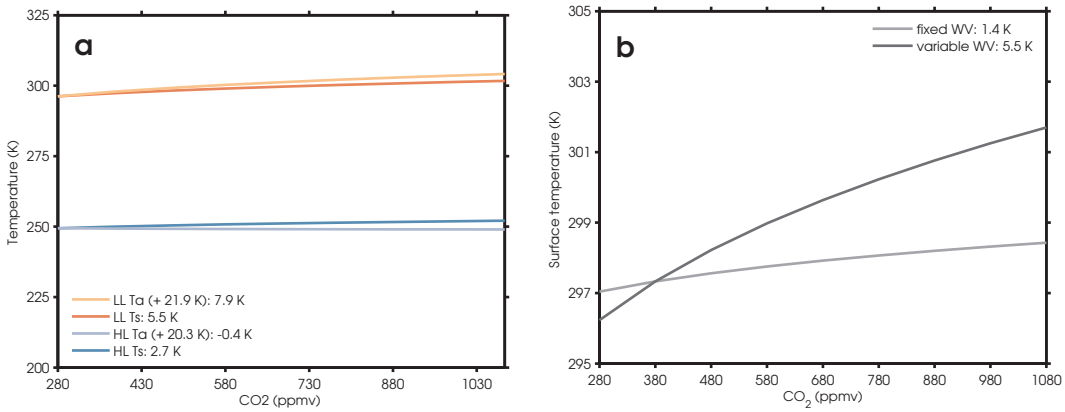

Figure 12: (a) (dark colors) Surface temperature and (light colors) atmospheric temperatures for the (orange) low- and (blue) high-latitudes in the column model with a multi-band radiative transfer scheme. (b) Comparison between the convective tropical surface temperature response to increasing CO_2 for a realistic radiative scheme with (light grey) moisture fixed to 380 ppmv levels and (dark grey) freely varying atmospheric moisture.